Observations of Multiple Nuclear Reaction Histories and Fuel-Ion Species Dynamics in Shock-Driven Inertial Confinement Fusion Implosions

H. Sio,[1,*] J. A. Frenje,[1] A. Le,[2] S. Atzeni,[3] T. J. T. Kwan,[2] M. Gatu Johnson,[1] G. Kagan,[2] C. Stoeckl,[4] C. K. Li,[1] C. E. Parker,[1] C. J. Forrest,[4] V. Glebov,[4] N. V. Kabadi,[1] A. Bose,[1] H. G. Rinderknecht,[4] P. Amendt,[5] D. T. Casey,[5] R. Mancini,[6] W. T. Taitano,[2] B. Keenan,[2] A. N. Simakov,[2] L. Chacón,[2] S. P. Regan,[4] T. C. Sangster,[4] E. M. Campbell,[4] F. H. Seguin,[1] and R. D. Petrasso[1]

[1]*Plasma Science and Fusion Center, Massachusetts Institute of Technology, Cambridge, Massachusetts 02139, USA*
[2]*Los Alamos National Laboratory, Los Alamos, New Mexico 87545, USA*
[3]*Dipartimento SBAI, Università degli Studi di Roma "La Sapienza," Via Antonio Scarpa 14, 00161, Roma, Italy*
[4]*Laboratory for Laser Energetics, Rochester, New York 14623, USA*
[5]*Lawrence Livermore National Laboratory, Livermore, California 94551, USA*
[6]*Physics Department, University of Nevada, Reno, Nevada, 89557, USA*

(Received 30 May 2018; revised manuscript received 27 August 2018; published 25 January 2019)

Fuel-ion species dynamics in hydrodynamiclike shock-driven DT^{3}He-filled inertial confinement fusion implosion is quantitatively assessed for the first time using simultaneously measured D^{3}He and DT reaction histories. These reaction histories are measured with the particle x-ray temporal diagnostic, which captures the relative timing between different nuclear burns with unprecedented precision (~10 ps). The observed 50 ± 10 ps earlier D^{3}He reaction history timing (relative to DT) cannot be explained by average-ion hydrodynamic simulations and is attributed to fuel-ion species separation between the D, T, and ^{3}He ions during shock convergence and rebound. At the onset of the shock burn, inferred ^{3}He/T fuel ratio in the burn region using the measured reaction histories is much higher as compared to the initial gas-filled ratio. As T and ^{3}He have the same mass but different charge, these results indicate that the charge-to-mass ratio plays an important role in driving fuel-ion species separation during strong shock propagation even for these hydrodynamiclike plasmas.

DOI: 10.1103/PhysRevLett.122.035001

Strong shocks are ubiquitous in inertial confinement fusion (ICF) [1] and many astrophysical plasmas [2], and the experimental results described in this letter may provide new insights into phenomena in these fields. Recent ICF experimental results reported increasing disagreements with average-ion-fluid simulations as ICF implosions become more kinetic [3,4], as well as indications of ion species separation and thermal decoupling [5]. However, thus far, these and other experimental results [6–10] have all relied on time-integrated nuclear observables such as yields and reaction temperatures. In experiment [11], Ar concentration change in a D-Ar mixture was observed using temporally and spatially resolved x-ray measurements; however, this technique cannot be applied to fuel ions such as D, T, or ^{3}He.

In contrast with previous studies that relied on time-integrated measurements, this letter presents the first time-resolved observation of fuel-ion species dynamics in ICF implosions using DT and D^{3}He reaction histories. These reaction histories were measured with the particle x-ray temporal diagnostic (PXTD) [12], which captures the relative timing between these reaction histories with unprecedented precision (~10 ps). These time-resolved measurements are contrasted with average-ion DUED [13] and multi-ion LSP [14] simulations. It is shown that the differential timing between reaction histories is a new manifestation of multi-ion dynamics, and that the difference between measured DT and D^{3}He reaction histories is consistent with rapidly changing fuel-ion composition caused by a strong shock in the central gas of an ICF target. Whereas previous ICF experiments in this plasma regime reported reasonable agreements with average-ion simulations using burn-averaged nuclear quantities [3], time-resolved reaction rates in this work clearly show differences between measurements and average-ion simulations not captured by time-integrated measurements.

Average-ion hydro simulations are essential for understanding and interpreting ICF implosions. For implosions with burn-averaged ion-ion mean free paths smaller than the burn radius, these simulations generally capture the implosion behaviors and burn-averaged quantities (yields, temperatures) [3], although not one-dimensional quantities like nuclear burn profiles [15]. Multi-ion dynamics, which are expected to impact and modify plasma conditions during the shock phase of ICF implosions [16–18], are approximately simulated in an *ad hoc* fashion in average-ion-fluid codes with additional physics models [19], as well as in kinetic-ion codes [20–23].

This experiment uses an exploding pusher platform [24], which is simple and ideal for studying the multi-ion dynamics during the shock phase in any ICF implosion. The reason for this is that shock phase plasma conditions (temperature, density, ion-ion mean-free-path, shock strength) are similar in all these implosions [3]. These exploding pusher targets are 860 μm in diameter with a 2.7-μm-thick SiO_2 shell. The gas-fill density is 2.2 mg/cc, with an atomic fuel composition of 49.6% D, 49.7% ^{3}He, and 0.7% T. These targets are driven symmetrically by sixty laser beams at the OMEGA laser facility [25] with a total energy of 14.4 kJ using a 0.6-ns-square pulse shape. These implosions are hydrodynamiclike, with $\lambda_{ii}/R_{\mathrm{burn}} \sim 0.3$, where λ_{ii} is the deuteron mean free path and R_{burn} is the fuel radius at peak burn.

These low-convergence (convergence ratio between 3 and 5), shock-driven implosions are not affected by hydrodynamic instabilities and mix [4]. On the other hand, SiO_2 from the shell could conceivably have been mixed into the gas from shock breakout across the fuel-shell interface. This scenario is very unlikely, as the absolute x-ray emissions measured by the hard x-ray detector [26] confirm an x-ray emission from a clean, mix-free D^{3}He fuel. The effect of spherically converging shock instability is expected to be negligible, as estimated using the analytical and numerical work by Gardner *et al.* [27]. Shock front deviation over the mean shock radius ($\delta r/r$) in this model increases with an amplitude given by $r^{-0.72}$ (for an ideal gas) as the shock converges. Given that laser illumination nonuniformity on target is less than 2% [28], and that initial local shock speed scales as the 1/3 power of the local laser intensity [29], the initial difference in local shock speed is ~0.7%. At a shock convergence of 20, $\delta r/r$ is only ~6%, or, a δr of 1 μm. Shock collapse and rebound further reduce $\delta r/r$ perturbations. In addition, experiments [30] with initial shock perturbations up to 14% show no difference in nuclear yields or timing during the shock phase.

The primary measurements in this experiment are the absolute DT and D^{3}He reaction histories, which are simultaneously measured with the PXTD. This is done by measuring the time-arrival histories of the monoenergetic 14.1-MeV DT-n and 14.7-MeV D^{3}He-p as they escape the implosion. As all measurements are made with the same diagnostic, the relative timing uncertainty between the DT and D^{3}He reaction histories is ~10 ps (versus ~40–50 ps, with the standard method of cross timing between two stand-alone diagnostics). This innovation is crucial to capturing the relative timing between different nuclear burns with sufficiently high precision to enable meaningful comparison between measurements and simulations.

The time period probed by the measured reaction histories in these ICF implosions is referred to as the shock phase. Nuclear yields are produced when the strong shock rebounds from the center of the implosion from the center of the implosion, increasing the fuel temperature and density. Figure 1 is a Lagrangian diagram from an average-ion DUED simulation for shot 82 615, showing the trajectories of fluid elements as a function of time. The shell trajectory (black data) as measured by an x-ray framing camera (XRFC) [31] agrees with the simulated shell trajectory. The measured DT and D^{3}He reaction rates provide information during the shock phase on the relative temporal differences between D, T, and ^{3}He temperature and density profiles through the following relations:

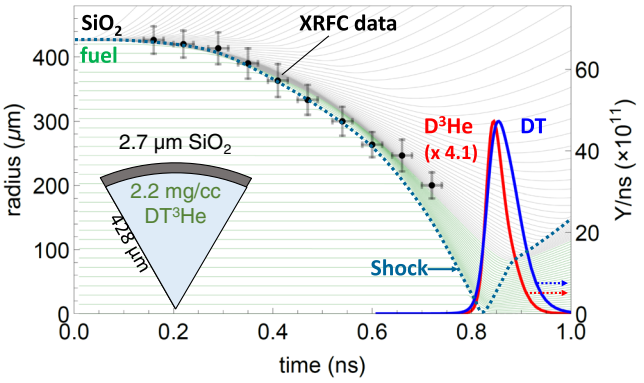

FIG. 1. Lagrangian diagram for OMEGA shot 82615 as simulated by the average-ion code DUED. The green (gray) lines denote the trajectories of fuel (shell) fluid elements as a function of time. The teal-dotted line is the shock trajectory. The DUED-simulated D^{3}He (red, ×4.1) and DT (blue) reaction histories are plotted to show nuclear reaction timing relative to shock convergence and rebound. The black data points are the measured shell locations at different times during the implosion.

$$Y_{\mathrm{D^3He}}(t)/s = \int n_{\mathrm{D}} n_{^3\mathrm{He}} \langle \sigma v \rangle_{\mathrm{D^3He}} (T_{i,\mathrm{D}}, T_{i,^3\mathrm{He}}) dV, \quad (1)$$

$$Y_{\mathrm{DT}}(t)/s = \int n_{\mathrm{D}} n_{\mathrm{T}} \langle \sigma v \rangle_{\mathrm{DT}} (T_{i,\mathrm{D}}, T_{i,\mathrm{T}}) dV, \quad (2)$$

where n is the ion number density, T_i is the ion temperature, and $\langle \sigma v \rangle$ is the Maxwellian-averaged reactivity. In the average-ion framework, n_{D}, n_{T}, and $n_{^3\mathrm{He}}$ are related by the initial gas-fill ratio, and the ion temperatures for all three ions ($T_{i,\mathrm{D}}$, $T_{i,\mathrm{T}}$, $T_{i,^3\mathrm{He}}$) are the same.

As time-resolved and time-integrated measurements are repeatable within uncertainty for four implosions (see Table I), shot 82 615 is used as a representative shot in this manuscript. Experimentally, the D^{3}He bang time is 50 ± 10 ps before the DT bang time [Fig. 2(a)], and is contrasted to the reaction histories as simulated by the average-ion hydrodynamic code DUED [Fig. 2(b)]. The DUED simulation used an electron flux limiter of 0.07, and included ion viscosity [32]. The DUED simulation also used a multigroup diffusive treatment of radiation transport and an equation-of-state [35]. For shot 82 615, the DUED-simulated D^{3}He, DT, and DD yields are 5.4×10^{10},

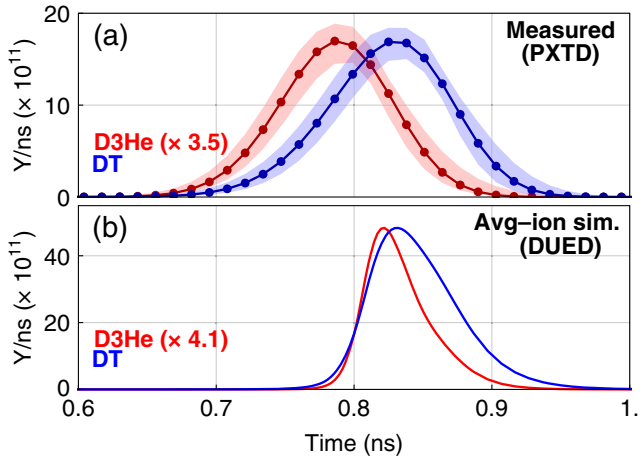

FIG. 2. (a) Absolute D^3He (red) and DT (blue) reaction histories measured by PXTD, and (b) simulated by DUED, for OMEGA shot 82 615. The magnitudes of the D^3He histories are scaled to match the DT histories for clarity in each case. Uncertainties in the PXTD data are indicated by the shaded regions.

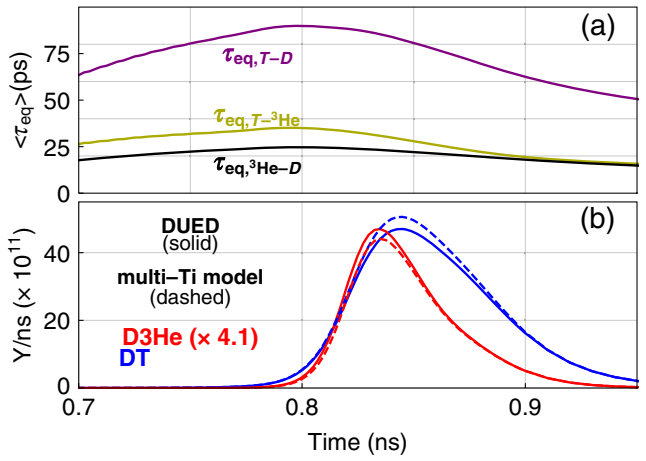

FIG. 3. (a) DUED-simulated, volume-averaged ion-ion thermalization time between T-D, T-^{3}He, and ^{3}He-D for shot 82 615. (b) DUED-simulated DT and D^3He reaction histories (blue-solid and red-solid lines, same as Fig. 2), and the resulting DT and D^3He reaction histories after post-processing the DUED simulation with a multi-Ti model (blue-dashed and red-dashed lines). The magnitudes of the D^3He histories (red-solid and red-dashed lines) are scaled by a factor of 4.1 for clarity.

3.7×10^{11}, and 7.0×10^{10}, respectively, comparable to the measured yields in Table I. The DUED-simulated burn-averaged D^3He, DT, and DD temperatures are 12.7, 11.0, and 10.4 keV, respectively, in good agreement with the measured temperatures. However, the average-ion DUED simulation cannot explain the relative timing between the measured D^3He and DT reaction histories, showing only a 10-ps timing difference between the two histories in the simulation. The DUED-simulated DT and D^3He burn widths are also more narrow as compared to the PXTD measurements.

In comparison with the average-ion simulation, a significantly higher D^3He reaction rate is observed relative to DT at the onset of the shock burn. This is observed on all four shots. Higher-than-expected ion temperature alone early in time in the fuel cannot explain this observation, as it would also have led to higher burn-averaged D^3He and DT temperatures, contrary to the measured burn-averaged temperatures.

The effect of different D, T, and ^{3}He temperatures cannot be ignored, but the effect is small according to DUED simulation post-processed with a multi-Ti model. Using this model, energy is partitioned to the D, T, and ^{3}He ions according to their masses, and temperatures are equilibrated using local plasma conditions. As expected from the short ion-ion thermalization time [Fig. 3(a)], the higher temperatures of the T and ^{3}He ions have a small impact on the reaction yields and, most importantly, have no effect on the timing of the reaction histories [Fig. 3(b)] [36].

However, the measured timing difference is consistent with ion species separation driven by sharp pressure gradients at the shock front [37] in the implosion. Explicitly calculating the ion diffusive flux (which depends on the charge and mass of the ion species) using expressions from [38] and gradients from the DUED simulation shows that the T ions are lagging behind the D and ^{3}He ions during shock convergence, consistent with the PXTD measurements. As the shock propagates radially inward, the diffusion coefficients at the shock front are $\sim 2 \times 10^3$ μm^2/ns, and the normalized pressure gradients

TABLE I. Experimental parameters and key observables. The absolute bang-time uncertainty (relative to the leading edge of the laser pulse) is 50 ps. The relative bang-time uncertainty (between D^3He and DT) is 10 ps. The uncertainties for the D^3He-p, DT, and DD yields are 20%, 5%, and 5%, respectively. The uncertainties for the D^3He-p, DT, and DD burn-averaged temperatures are 1.5, 0.5, and 0.5 keV, respectively.

Shot	Gas-fill atm	Laser kJ	Bang time (ps)		Yield			Ti (keV)		
			D^3He	DT	D^3He	DT	DD	D^3He	DT	DD
82 613	$D_2[4.9]T_2[0.07]^3He[9.3]$	14.3	755	809	4.0×10^{10}	1.7×10^{11}	...	13.9	...	...
82 614	$D_2[4.9]T_2[0.07]^3He[9.7]$	14.2	800	841	4.9×10^{10}	2.0×10^{11}	4.0×10^{10}	15.0	11.0	11.6
82 615	$D_2[4.9]T_2[0.07]^3He[9.8]$	14.2	780	831	5.2×10^{10}	1.9×10^{11}	3.8×10^{10}	12.6	10.7	10.5
82 616	$D_2[4.9]T_2[0.07]^3He[9.8]$	14.1	840	875	4.0×10^{10}	2.0×10^{11}	3.7×10^{10}	11.1	10.9	11.1

$(\nabla P/P)$ are $\sim 0.2\ \mu\mathrm{m}^{-1}$. These terms lead to an ion diffusive flux of $\sim 300\ \mu$m/ns in the shock frame. The dominant terms driving the D and ^{3}He ions forward relative to the T ions are from the ion pressure gradient (barodiffusion, which accelerates the lighter D ions ahead) and the electron pressure gradient (electrodiffusion, which accelerates the higher-charge ^{3}He ions ahead).

As temperature effects are demonstrably small, the observed difference between the measured reaction histories is attributed to fuel-ion-species separation between the D, T, and ^{3}He ions. To infer the level of separation in the burn region needed to explain the measured reaction histories, the ratio of Eqs. (1) and (2) is approximated as

$$\frac{Y_{\mathrm{D^3He}}(t)/s}{Y_{\mathrm{DT}}(t)/s} \approx \frac{\langle n_{^3\mathrm{He}}\rangle}{\langle n_{\mathrm{T}}\rangle}\frac{\langle \sigma v\rangle_{\mathrm{D^3He}}}{\langle \sigma v\rangle_{\mathrm{DT}}}, \tag{3}$$

where n is the ion number density for the different ion species and $\langle \sigma v\rangle$ is the Maxwellian-averaged reactivity for the different reactions. This approximation for the instantaneous D^{3}He/DT yield ratio is valid if the ion temperature variance over the burn region is small [10], which is the case for these hydrodynamiclike implosions. Calculating Eq. (3) and the exact ratio explicitly in simulation shows that this approximation introduces less than 20% uncertainty.

The measured D^{3}He and DT reaction histories in Fig. 2(a) are used to obtain the instantaneous D^{3}He/DT yield ratio in Fig. 4(a). Using Eq. (3), the burn-averaged ^{3}He/T fuel ratio in the burn region as a function of time [Fig. 4(b)] is inferred from the measured instantaneous D^{3}He/DT yield ratio. The horizontal purple-dashed line indicates the initial ^{3}He/T gas-fill ratio. The reactivity ratio is extracted from the average-ion simulation and is constrained by measured DD, DT, and D^{3}He ion temperatures.

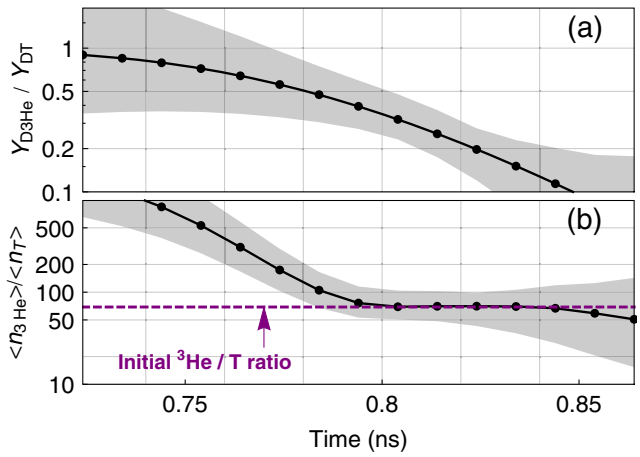

FIG. 4. (a) instantaneous D^{3}He/DT yield ratio for shot 82 615. In (b), the inferred $\langle n_{^3\mathrm{He}}\rangle/\langle n_{\mathrm{T}}\rangle$ (black data) is plotted. The purple-dashed line marks the initial ^{3}He/T fuel ratio. Uncertainties in the data are indicated by the shaded regions.

At the onset of the shock burn, the inferred ^{3}He/T fuel ratio in the burn region is much higher as compared to the initial ^{3}He/T gas-fill ratio in all implosions. The relaxation of $\langle n_{^3\mathrm{He}}\rangle/\langle n_{\mathrm{T}}\rangle$ toward initial gas-fill ratio is partially a consequence of the burn region expanding outward and encompassing a larger fraction of the fuel volume as the shock rebounds.

It is also insightful to illustrate the evolution of the D, T, and ^{3}He ion density profiles evolution in an ICF implosion using a simulation code that treats the D, T, and ^{3}He ion population separately. The particle-in-cell code LSP is used to simulate OMEGA shot 82 615, treating the D, T, ^{3}He, and SiO_2 ion species as kinetic. The electrons are treated as a fluid. More details on the LSP simulation method can be found in [39,40]. The LSP simulation is initiated at $t = 0.55$ ns using initial conditions from a hydrodynamic simulation shortly after the shock breaks out from the shell (see Fig. 1). The LSP-simulated implosion trajectory agrees with DUED simulation and XRFC data (Fig. 1).

At $t = 0.66$ ns (Fig. 5), 110 ps after LSP initialization, fuel-ion species separation has already developed between the D, T, and ^{3}He ions. As the shock rebounds from the center ($t = 0.76$ ns), the temperature profiles are centrally peaked. The fusion reactivities' dependence on temperature weights the DT and D^{3}He reaction profiles toward the center of the implosion. However, because the T ion number density profile is skewed toward the outer volume of the fuel that is not yet heated by the rebounding shock, the D^{3}He yield is higher than DT yield at this early time, relative to average-ion simulation, leading to an earlier D^{3}He reaction history relative to DT (see Fig. 6) that is consistent with the PXTD measurements in Fig. 2. The LSP-simulated D^{3}He burn width is consistent with the PXTD measurements, while the LSP-simulated DT burn width is

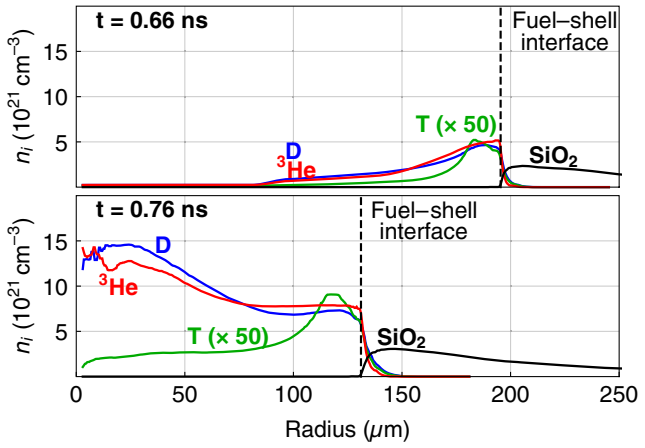

FIG. 5. LSP-simulated ion number density profiles at $t = 0.66$ ns (shock converging) and $t = 0.76$ ns (shock rebounding). The D, T, and ^{3}He ion number densities are plotted in blue, green, and red, respectively. The number density profile for the T ions has been scaled by 50 for clarity. The vertical black-dashed line denotes the fuel-shell interface.

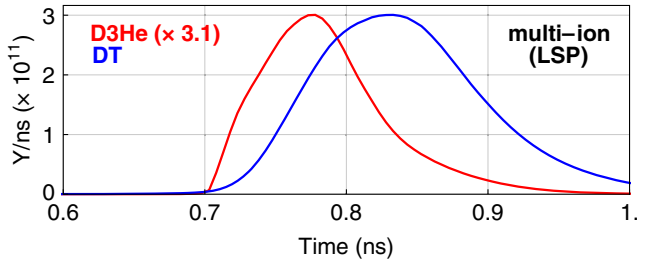

FIG. 6. LSP-simulated DT (blue) and D^{3}He (red) reaction histories for shot 82 615. The magnitude of the D^{3}He reaction history is scaled by a factor of 3.1 for clarity. The absolute magnitude of the LSP-simulated reaction histories is notably lower than the measurements, in part because of the reduced laser coupling in the simulation [40].

notably wider. Qualitatively, this LSP simulation clearly demonstrates how fuel-ion species separation that developed during shock propagation and rebound manifest as a timing differential between reaction histories. In addition, the effects of non-Maxwellian distribution (fast ions, etc.) have been captured by the LSP simulations.

In summary, the timing difference between measured DT and D^{3}He reaction histories in hydrodynamiclike shock-driven implosions cannot be explained by average-ion simulations and is attributed to ion species separation between the D, T, and ^{3}He ions during shock convergence and rebound. At the onset of the shock burn, the ^{3}He/T fuel ratio in the burn region inferred from the measured reaction histories is much higher as compared to the initial ^{3}He/T gas-fill ratio, in contrast with average-ion simulations. As T and ^{3}He have the same mass but a different charge, these results indicate that the charge-to-mass ratio plays an important role in driving fuel-ion species separation during strong shock propagation. It is unclear how these multi-ion effects affect implosion performance during the deceleration and compression phase, as existing experimental results [6–10] have been mixed. Future work includes quantifying these effects in very hydrodynamic shock-driven implosions (Very hydrodynamic implosions have occurred on the NIF [41], but the NIF facility lacks a PXTD-type diagnostic and capability described herein.); in very kinetic implosions; in the ablative phase of compressive implosions; and in astrophysical settings such as SN 1987a [2], where non-equilibrium kinetic effects and signatures (such as temperature differences between ion species) could be present.

The authors thank A. Birkel, R. Frankel, and E. Doeg for contributing to the fielding and processing of CR-39 data used in this work, Bruce Remington for helpful discussions, as well as the OMEGA operations crew for their help in executing these experiments. The targets and gas fills are coordinated by GA and the LLNL and LLE tritium facilities. This material is based upon work supported by the Department of Energy, National Nuclear Security Administration under Awards No. DE-NA0001857, No. DE-NA0002949, and No. DENA0002905. The work was also supported in part by National Laser User's Facility (Grant No. DE-NA0002035). H. S. was supported by the DOE NNSA SSGF (Grant No. DE-FC52-08NA28752) during this work. S. A. acknowledges Sapienza Projects No. 2015 C26A15YTMA and No. 2016-257584, as well as EUROfusion Project No. AWP17-ENR-IFE-CEA-01. G. K. and A. L. acknowledge the LANL LDRD Program. This report was prepared as an account of work sponsored by an agency of the United States Government. Neither the United States Government nor any agency thereof, nor any of their employees, makes any warranty, express or implied, or assumes any legal liability or responsibility for the accuracy, completeness, or usefulness of any information, apparatus, product, or process disclosed, or represents that its use would not infringe privately owned rights. The views and opinions of authors expressed herein do not necessarily state or reflect those of the United States Government or any agency thereof.

*hsio@mit.edu

[1] J. Lindl *et al.*, Phys. Plasmas **11**, 339 (2004).
[2] S. Park, S. A. Zhekov, D. N. Burrows, G. P. Garmire, and R. McCray, Astrophys. J **610**, 275 (2004).
[3] M. J. Rosenberg *et al.*, Phys. Rev. Lett. **112**, 185001 (2014).
[4] H. G. Rinderknecht *et al.*, Phys. Rev. Lett. **112**, 135001 (2014).
[5] H. G. Rinderknecht *et al.*, Phys. Rev. Lett. **114**, 025001 (2015).
[6] J. R. Rygg *et al.*, Phys. Plasmas **13**, 052702 (2006).
[7] H. W. Herrmann *et al.*, Phys. Plasmas **16**, 056312 (2009).
[8] D. T. Casey *et al.*, Phys. Rev. Lett. **108**, 075002 (2012).
[9] C. J. Forrest, P. B. Radha, J. P. Knauer, V. Yu. Glebov, V. N. Goncharov, S. P. Regan, M. J. Rosenberg, T. C. Sangster, W. T. Shmayda, C. Stoeckl, and M. G. Johnson, Phys. Rev. Lett. **118**, 095002 (2017).
[10] D. T. Casey *et al.*, Nat. Phys. **13**, 1227 (2017).
[11] S. C. Hsu *et al.*, Europhys. Lett. **115**, 65001 (2016).
[12] H. Sio *et al.*, Rev. Sci. Instrum. **87**, 11D701 (2016).
[13] S. Atzeni, A. Schiavi, F. Califano, F. Cattani, F. Cornolti, D. Del Sarto, T. V. Liseykina, A. Macchi, and F. Pegoraro, Comput. Phys. Commun. **169**, 153 (2005).
[14] D. R. Welch, D. V. Rose, R. E. Clark, T. C. Genoni, and T. P. Hughes, Comput. Phys. Commun. **164**, 183 (2004).
[15] M. J. Rosenberg *et al.*, Phys. Plasmas **22**, 062702 (2015).
[16] P. Amendt, O. L. Landen, H. F. Robey, C. K. Li, and R. D. Petrasso, Phys. Rev. Lett. **105**, 115005 (2010).
[17] G. Kagan and X.-Z. Tang, Phys. Plasmas **19**, 082709 (2012).
[18] H. G. Rinderknecht, P. A. Amendt, S. C. Wilks, and G. Collins, Plasma Phys. Controlled Fusion **60**, 064001 (2018).
[19] N. Hoffman *et al.*, Phys. Plasmas **22**, 052707 (2015).
[20] C. Bellei, P. A. Amendt, S. C. Wilks, M. G. Haines, D. T. Casey, C. K. Li, R. Petrasso, and D. R. Welch, Phys. Plasmas **20**, 012701 (2013).

[21] C. Bellei, H. Rinderknecht, A. Zylstra, M. Rosenberg, H. Sio, C. K. Li, R. Petrasso, S. C. Wilks, and P. A. Amendt, Phys. Plasmas **21**, 056310 (2014).
[22] W. T. Taitano, L. Chacón, A. N. Simakov, and K. Molvig, J. Comput. Phys. **297**, 357 (2015).
[23] O. Larroche, H. G. Rinderknecht, M. J. Rosenberg, N. M. Hoffman, S. Atzeni, R. D. Petrasso, P. A. Amendt, and F. H. Séguin, Phys. Plasmas **23**, 012701 (2016).
[24] M. D. Rosen *et al.*, Phys. Fluids **22**, 1393 (1979).
[25] T. R. Boehly *et al.*, Opt. Commun. **133**, 495 (1997).
[26] C. Stoeckl, V. Yu. Glebov, D. D. Meyerhofer, W. Seka, B. Yaakobi, R. P. J. Town, and J. D. Zuegel, Rev. Sci. Instrum. **72**, 1197 (2001).
[27] J. Gardner, D. L. Book, and I. B. Bernstein, J. Fluid Mech. **114**, 41 (1982).
[28] F. J. Marshall, J. A. Delettrez, R. Epstein, R. Forties, R. L. Keck, J. H. Kelly, P. W. McKenty, S. P. Regan, and L. J. Waxer, Phys. Plasmas **11**, 251 (2004).
[29] J. Lindl, Phys. Plasmas **2**, 3933 (1995).
[30] J. R. Rygg, J. A. Frenje, C. K. Li, F. H. Séguin, R. D. Petrasso, F. J. Marshall, J. A. Delettrez, J. P. Knauer, D. D. Meyerhofer, and C. Stoeckl, Phys. Plasmas **15**, 034505 (2008).
[31] D. K. Bradley, P. M. Bell, O. L. Landen, J. D. Kilkenny, and J. Oertel, Rev. Sci. Instrum. **66**, 716 (1995).
[32] Two other 1D radiation-hydrodynamic codes, LILAC [33] and HYADES [34], are used to simulate these implosions, with similar results. DUED has also been extensively benchmarked against LILAC and HYADES in Ref. [3].
[33] J. A. Delettrez, R. Epstein, M. C. Richardson, P. A. Jaanimagi, and B. L. Henke, Phys. Rev. A **36**, 3926 (1987).
[34] J. T. Larsen and S. M. Lane, J. Quant. Spectrosc. Radiat. Transfer **51**, 179 (1994).
[35] S. Atzeni, A. Caruso, and V. A. Pais, Laser Part. Beams **4**, 393 (1986).
[36] The effective DT and D^3He fusion temperatures for two Maxwellian ion populations are given by [21] $T_{\mathrm{fus,DT}} = (m_{\mathrm{T}}T_{i,\mathrm{D}} + m_{\mathrm{D}}T_{i,\mathrm{T}})/(m_{\mathrm{D}} + m_{\mathrm{T}})$ and $T_{\mathrm{fus,D^3He}} = (m_{^3\mathrm{He}}T_{i,\mathrm{D}} + m_{\mathrm{D}}T_{i,^3\mathrm{He}})/(m_{\mathrm{D}} + m_{^3\mathrm{He}})$, respectively, where m is the ion mass and T_i is the ion temperature for each ion species.
[37] G. Kagan and X.-Z. Tang, Phys. Lett. A **378**, 1531 (2014).
[38] G. Kagan *et al.*, arXiv:1611.09872.
[39] A. Le *et al.*, Phys. Plasmas **23**, 102705 (2016).
[40] As the laser pulse is truncated once, the LSP simulation begins, 30% less laser energy is coupled to the target in the LSP simulation. The reduced laser coupling is not the cause of the timing difference between the DT and D^3He reaction histories, as hydrodynamic simulations ran with full laser coupling and reduced laser couplings have the same timing difference.
[41] S. LePape *et al.*, Phys. Rev. Lett. **112** ,225002 (2014).